Academic Journal of Applied Sciences
ISSN: 3105-0549 (Print), ISSN: 3105-0557 (Online) | Vol. 1, No. 1, 2026

Fusing Optical Remote Sensing and SAR Garlic Planting Structure Extraction Method

Yanan Wang, Xiaoping Lu

School of Surveying and Land Information Engineering, Henan Polytechnic University, Jiaozuo 454000, China

Abstract: Obtaining crop planting structure information is an important basis for agricultural production management and policy formulation. As an important economic crop in China, high-precision identification of garlic planting distribution is of great significance for production management, optimization of planting structure, and yield assessment. Addressing the problems of mixed pixels and spectral confusion caused by the overlapping growth periods of garlic and winter wheat, and the small and scattered planting plots, this study takes Kaifeng City in Henan Province as the research area, integrating Sentinel-2 optical images and Sentinel-1 radar data, and conducts garlic planting distribution identification based on phenological features. The main results are as follows: (1) A multimodal time-series vegetation index dataset for the entire growth period of garlic was constructed, and after smoothing by Savitzky–Golay filtering, a continuous and stable vegetation index variation curve was obtained to identify key turning points for dividing critical phenological periods. (2) To address the problem that optical data is easily affected by weather, a method integrating optical and SAR data was proposed, extracting optical and radar features at different phenological periods to construct optimal recognition features. Classification results show that after integrating optical and SAR data with phenological information, the overall accuracy reached 96.27%, with a Kappa coefficient of 0.95. This method effectively overcomes the problems of spectral confusion and mixed pixels in garlic identification, significantly improves classification accuracy and spatial consistency, and provides effective technical support for the accurate acquisition of garlic planting structure information.

Keywords: Temporal analysis; Multimodal remote sensing; Planting structure; Phenological period; Growth characteristics.

1. Introduction

Garlic is an important economic crop. According to the statistics database of the Food and Agriculture Organization (FAO) of the United Nations, since 2016, China's garlic production has steadily increased, making it the world's largest producer, accounting for more than 70% of the world's production annually. There is a global imbalance in garlic supply and demand (FAO 2022) [1]. Therefore, obtaining accurate information on garlic distribution not only helps improve regional crop management but also has important significance for optimizing yield models. Traditional garlic planting area surveys rely on field sampling techniques, which are characterized by high cost, long sampling cycles, and challenges in providing timely information on garlic planting[2]. The maturity of the remote sensing industry provides a solution, enabling fast, large-scale, and cost-effective monitoring of garlic planting through satellite remote sensing data [3].

Currently, optical remote sensing and synthetic aperture radar (SAR) are the two most commonly used data sources in crop classification research[4]. Optical remote sensing images can sensitively capture vegetation spectral characteristics, thus having an intuitive advantage in characterizing crop growth status and distinguishing different crop types[5]. However, optical images are highly susceptible to weather and clouds, especially in winter and rainy areas, often resulting in time series gaps and incomplete information. In comparison, SAR images do not rely on sunlight, can stably acquire data under both day and night as well as cloudy conditions, and their signals are highly sensitive to crop canopy structure, soil moisture, and roughness, which can complement the shortcomings of optical data. SAR data itself has strong speckle noise, which can easily cause a 'salt-and-pepper effect' in classification results, affecting spatial continuity and mapping accuracy [6]. Therefore, the complementary advantages of optical remote sensing and SAR data have become an important direction in crop classification research in recent years. Many studies have shown that integrating active and passive remote sensing data can significantly improve classification accuracy and robustness[7].

Based on the above issues, this study proposes a Phenology-based Passive and SAR Feature (PPSF) method and applies it to garlic classification in Kaifeng City. This method integrates optical and SAR time series data and conducts classification experiments based on phenological features. During this process, we attempt to address the limitations of using fixed windows to divide phenological periods and explore the role of multi-phenological-responsive features in crop identification. The research results provide new ideas for high-precision remote sensing mapping of garlic and have reference significance for the classification studies of other small-plot economic crops.

2. Research Area and Data Sources

2.1. Overview of the Research Area

The study area is Kaifeng City, Henan Province (113°52′15″–115°15′42″ E, 34°11′45″–35°01′20″ N), located in the eastern Henan Plain, with flat terrain and an elevation of about 68–78 m, covering a total area of approximately 6,240 km² (Figure 1). The area has a warm temperate continental monsoon climate, with an annual average temperature of about 14.5 °C and annual precipitation of approximately 627–663 mm, concentrated in the summer (July–September). This climate is suitable for the growth of various crops. Garlic is a characteristic economic crop of this region. According to the Henan Statistical Yearbook, the planting area remained above 590 km² from 2021 to 2023, accounting for 20% of the province's total garlic planting area. The garlic sowing period in this area is in late September, and the harvest period is from May to June of the following year. The growth stages of winter wheat and garlic are similar, which brings difficulties for garlic mapping.

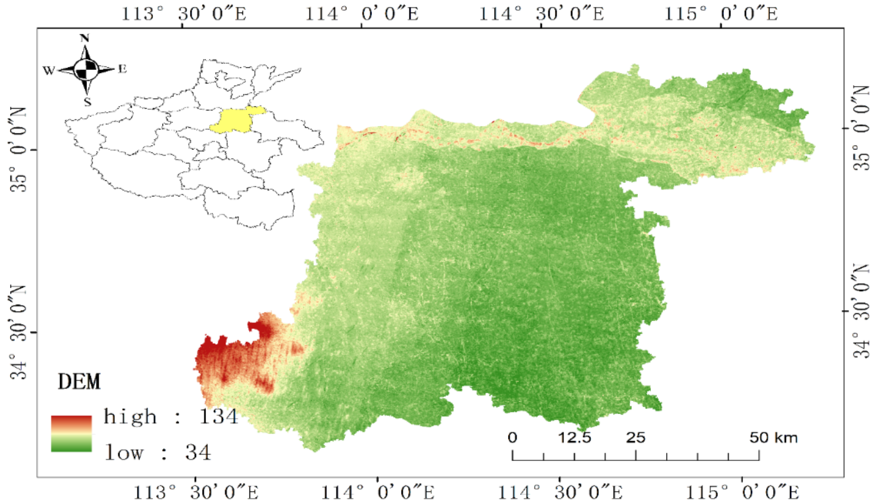

Fig. 1 Location Map of the Study Area

2.2. Dataset and Preprocessing

This study completed the acquisition, preprocessing, feature extraction, and final classification of remote sensing images based on the Google Earth Engine (GEE) platform[8]. GEE is a cloud-based processing platform for geospatial analysis developed by Google. Because it integrates massive remote sensing and geographic data products, provides powerful distributed computing capabilities, and offers a variety of image processing algorithms, it can support rapid processing and analysis of large-scale spatiotemporal data[9,10].

2.2.1. Sentinel-2 Data

Sentinel-2 MSI multispectral data is provided by the European Space Agency (ESA), including images from the S2A and S2B satellites. The revisit period of a single satellite is 10 days, and the combination of both satellites can achieve a revisit period of approximately 5 days[11,12]. A total of 318 high-quality L2A multispectral images covering the period from September 20, 2023, to June 11, 2024, were selected as the research data.

2.2.2. Sentinel-1 Data

Sentinel-1 SAR active microwave data is provided by ESA and includes images from the S1A and S1B satellites. The revisit period for a single satellite is 12 days, and the combination of the two satellites can achieve a revisit frequency of about 6 days[13]. Considering the growth season and phenological characteristics of garlic, we selected 64 high-quality images covering the study area from September 20, 2023, to June 11, 2024. These images, through their interaction with crop structure and moisture, can provide information that is different from and complementary to optical images for crop classification.

2.2.3. Ground Reference Data

The field survey data for this study were collected in 2024, covering garlic, wheat, and other crops. A total of 363 garlic sample points, 246 wheat sample points, 219 building sample points, 233 other vegetation sample points, and 142 water sample points were collected. All sample points underwent spatial filtering in GEE to remove points within 100 meters of each other. Their spatial distribution is shown in Figure 1b. Among them, 110 garlic sample points were used for identifying regional adaptive phenological stages, while the remaining training and validation samples were allocated in a 7:3 ratio. The results are shown in Table 1.

Table 1. Table1 Sample data sets

Date category	Garlic	Winter wheat	Built-up	Other vegetation	Water	Total
Training datasets	174	171	156	174	96	741
Verification datasets	79	75	63	59	46	352
Total	253	246	219	142	142	1093

3. Research Methods

3.1. Regional Adaptive Phenology Recognition

3.1.1. Time Series Generation

To avoid the impact of insufficient imagery at the beginning and end of the growing season on phenology recognition, this study collected Sentinel-1 and Sentinel-2 remote sensing observation data from August 1, 2023, to August 1, 2024, with DOY0 being August 1, 2023. From 329 garlic sample points, 110 were randomly selected for time series construction. Scatter plots were generated using the median of sample point observations within a five-day time window (as shown in Figure 2), and outliers were removed using the mean ± 2 standard deviations method. The median time series was retained as input. To ensure the sensitivity of the original curves, no interpolation was performed; instead, the median curves were smoothed using the Savitzky–Golay filter to generate vegetation index time series curves, with the blue band representing ±1.5σ fluctuation range. The Savitzky–Golay filter is a commonly used digital filtering technique for smoothing vegetation time series noise, which removes noise while preserving the original trend through local polynomial fitting[14]. As for Sentinel-1 data, after applying radiometric calibration and Refined Lee filtering, the median of sample points was calculated over six-day periods, without interpolation, and outlier smoothing was achieved using the Savitzky–Golay filter. Using the median instead of the mean can reduce the influence of extreme values and better preserve the representative values of the vegetation index or backscatter.

3.1.2. Phenological Stage Division

To improve the reliability of phenological division, we constructed six multi-source optical and SAR time series, namely BSI, VV/VH, NDVI, LSWI, GCVI, and PSRI, based on which six key phenological stages were identified (mulching–sowing period, germination period, seedling period, overwintering period, regreening–rapid growth period, and maturity period). The reasons for selecting these indices include: (1) BSI effectively represents soil minerals during the bare soil period and monitors soil exposure[15]; (2) Ali et al. (2019), in their study on winter wheat in Lebanon, found that the first peak of the Sentinel-1 VV/VH curve fitted with a Gaussian function had an estimation error of only −0.2 days for the germination period [9]. Since garlic and winter wheat are both winter crops with similar growth trends, this study used the same method to identify the garlic germination period (Figure 2b), effectively improving classification accuracy[16]; (3) NDVI is a widely recognized vegetation-sensitive index. In the early crop growth stage, development is relatively slow, which avoids misclassification risks and saturation problems[17]; (4) LSWI is particularly sensitive to vegetation and surface moisture changes, allowing monitoring of humidity during overwintering[18]; (5) GCVI was chosen to monitor the regreening–rapid growth period because it can estimate chlorophyll content[19]; (6) PSRI can reflect carotenoid content and leaf senescence during the maturity period . Moreover, combining optical and microwave time series allows mutual verification, reducing the impact of weather on optical imagery and effectively improving the robustness of phenological division.

Based on Figure 2 and the phenological knowledge of garlic growth, the entire growth cycle is divided into six key phenological stages:

(1) Mulching–sowing period (DOY 50–70): BSI remains high, indicating surface cover or exposed bare soil; NDVI is low at the same time, showing that green vegetation has not yet emerged, thus confirmed as the mulching–sowing period.

(2) Germination period (DOY 70–85): VV/VH reaches the first peak, reflecting roughness changes caused by emerging buds and leaves; LSWI shows no obvious water surge, excluding interference from rainfall or irrigation; NDVI starts to rise gradually, indicating the initial appearance of green vegetation, thus defined as the germination period.

(3) Seedling period (DOY 85–115): Leaves expand rapidly, NDVI reaches its first peak, and BSI shows a concurrent trough, indicating the surface is covered by green plants, confirming entry into the seedling period.

(4) Overwintering period (DOY 115–205): LSWI first rises and then falls, consistent with the common practice of applying overwintering water during garlic cultivation in Kaifeng; NDVI shows a plateau, reflecting growth stagnation, thus defined as the overwintering period.

(5) Regreening–rapid growth period (DOY 205–260): GCVI rises significantly due to chlorophyll accumulation; NDVI rises synchronously, while PSRI remains low, indicating entry into the vigorous growth period.

(6) LS: PSRI continues to rise, reflecting an increase in carotenoid content and leaf senescence; a decline in NDVI indicates a maturity stage signal.

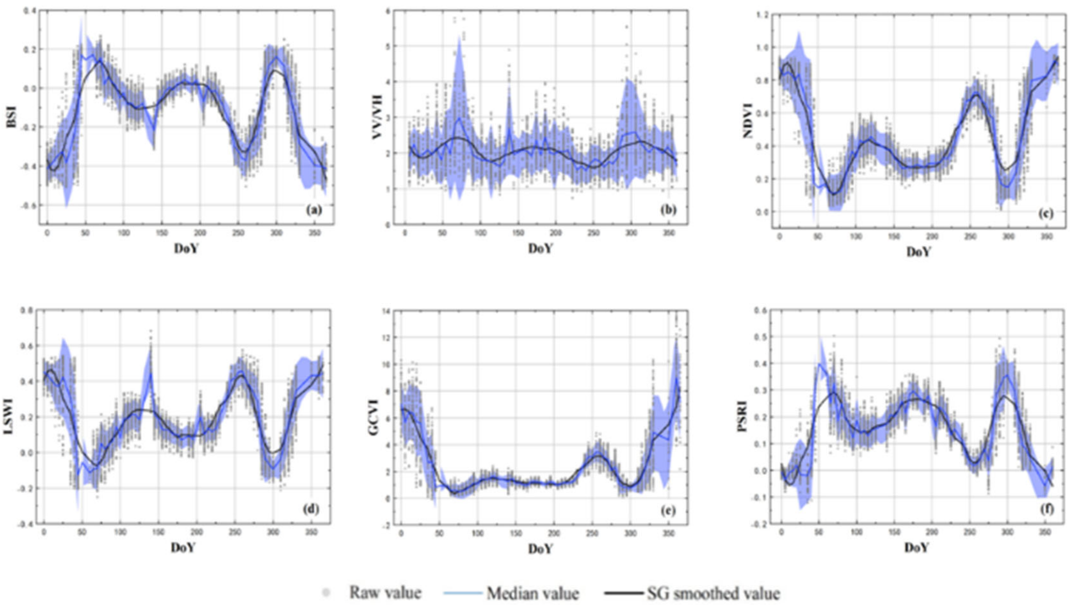

Fig. 2 Spectral indices temporal profiles. Subfigure (a), (b), (c), (d) , (e)and (f)are BSI, VV/VH,NDVI,LSWI, GCVI, and PSRI, respectively.

3.2. Extraction of Stage-Specific Passive and Active Sensitive Features

In this study, the garlic growth cycle was first divided into six phenological stages: PP1 (mulching–sowing), PP2 (germination), PP3 (seedling), PP4 (overwintering), PP5 (regreening–rapid growth), and PP6 (maturity). Then, based on the sensitivity of features at each stage, different passive and active features were extracted from images corresponding to each time period using a median synthesis method as the final features (see Table 2).

The logic for selecting stage-sensitive feature combinations is as follows:

PP1: BSI is used to capture the strong reflectance difference between bare soil and mulch, supplemented by SAVI to enhance the perception of early greenness differences while reducing soil background interference, and NDVI is introduced to perform baseline monitoring of initial coverage.

PP2: VV/VH is used to capture roughness changes as buds and leaves emerge from the soil, with VV polarization signal added to enhance sensitivity to moisture and structural details during the germination stage.

PP3: NDVI is used to describe leaf coverage growth, coupled with NDBI to suppress interference from bare soil and buildings, while GNDVI (using the difference between green and near-infrared light) is introduced to enhance detection of early leaf expansion and chlorophyll accumulation.

PP4: LSWI represents water dynamics during overwintering, supplemented by VH to capture winter canopy structure and moisture characteristics.

PP5: GCVI reflects chlorophyll accumulation and regreening stage, supplemented by S2REP to quantify red-edge shift, strengthening the detection of canopy structure and physiological changes.

PP6: PSRI is chosen to capture leaf yellowing signals during maturity, combined with MSI to monitor moisture stress trends, with NDRE additionally introduced to enhance detection of red-edge pigment changes in leaves, thereby enabling identification of physiological senescence during the maturity stage.

This combination strategy not only leverages the validated advantages of existing indices in garlic phenology analysis but also compensates for blind spots caused by single indices, such as recognition errors and background interference. The introduction of VARI significantly improves identification in areas with mixed bare soil and weeds. Overall, stage-sensitive feature design provides more comprehensive and stable recognition capability for classification. Table 3 shows the results of passive and active sensitive feature extraction for the six phenological stages.

Table 2. Sensitive Features of Garlic in Six Phenological Stages

Phenological Stage	Sensitive Features (Optical & SAR)	Expression
Mulching–Sowing Stage	BSI, SAVI, NDVI	PP1
Germination Stage	VV/VH, VV	PP2
Seedling Stage	NDVI, NDBI, GNDVI	PP3
Overwintering Stage	LSWI, VH	PP4
Regreening–Rapid Growth Stage	GCVI, S2REP	PP5
Maturity Stage	PSRI, MSI, NGRPI	PP6

3.3. JM Spectral Separability

Since prior experiments showed that wheat has the highest confusion rate with garlic, this study focuses on evaluating the spectral separability between garlic and wheat. In this study, the Jeffries–Matusita (JM) distance was used for measurement, and separability is defined as follows:

It is the Bhattacharyya distance, calculated by the formula:

$$J-M=2(1-e^{-Bij}) \tag{1}$$

$$Bij=\frac{1}{8}(\mathrm{m_i}-\mathrm{m_j})\frac{2}{\sigma_i^2+\sigma_j^2}+\frac{1}{2}\ln\left(\frac{2\sigma_i^2+\sigma_j^2}{2\sigma_i^2\sigma_j^2}\right) \tag{2}$$

In this formula, JM represents the J-M distance between categories i and j, Bij represents the corresponding Bhattacharyya distance; mi and mj represent the mean vectors of features for categories i and j, respectively, and Σi and Σj represent the corresponding covariance matrices. These statistical parameters describe the distribution of samples from different categories in the feature space and further calculate their degree of separability. The JM distance ranges from 0 to 2, with larger values indicating stronger separability.

To verify the improvement of the stage-sensitive feature scheme on classification, we compared the combination of single-phenological-stage primary active features with cumulative stage-wise addition. The stage-sensitive feature combinations for each stage are shown in Table 3.

Table 3. Combinations of Phenological Stages and Corresponding Sensitive Features

The combinations of phenological periods	Sensitive Features	Expression
PP1	BSI, SAVI, NDVI	PP1
PP2	VV/VH, VV	PP2
PP3	NDVI, NDBI, GNDVI	PP3
PP4	LSWI, VH	PP4
PP5	GCVI, S2REP	PP5
PP6	PSRI, MSI, NGRPI	PP6
PP1, PP2	BSI, SAVI, NDVI, VV/VH, VV	PP1-2
PP1, PP2, PP3	BSI, SAVI, NDVI, VV/VH, VV,	PP1-3
	NDVI, NDBI, GNDVI	
PP1, PP2, PP3, PP4	BSI, SAVI, NDVI, VV/VH, VV,	PP1-4
	NDVI, NDBI, GNDVI, LSWI, VH	
PP1, PP2, PP3, PP4, PP5	BSI, SAVI, NDVI, VV/VH, VV,	PP1-5
	NDVI, NDBI, GNDVI, LSWI, VH,	
	GCVI, S2REP	
PP1, PP2, PP3, PP4, PP5, PP6	BSI, SAVI, NDVI, VV/VH, VV,	PP1-6
	NDVI, NDBI, GNDVI, LSWI, VH,	
	GCVI, S2REP, PSRI, MSI, NDRE	

3.4. Phenology-Driven Classification Model and Evaluation

Random Forest is an ensemble learning algorithm proposed by Breiman and others, consisting of multiple decision trees, and determining the final class through voting on the classification results of each tree. In this study, the Random Forest algorithm was selected to classify garlic planting areas. Preliminary experiments showed that when the number of decision trees was set to 100, the model results were relatively stable, and dividing the training and testing sets at a 7:3 ratio could achieve better performance. To assess the impact of different data source combinations and the introduction of phenology information on garlic classification, five comparative models were designed, including factors such as whether to include phenology-sensitive features and whether to integrate active and passive remote sensing data (Table 4). Among them, Models 1-3 are based on annual data, using radar, optical, and active-passive fused monthly composite features, without introducing phenology-sensitive information; Models 4 and 5 introduce six phenological periods, constructing phenology-sensitive feature models based on optical data and active-passive fused data, respectively. This allows a systematic assessment of the impact of phenology-sensitive features and multi-source data fusion on classification.

The performance evaluation of the classification results includes both qualitative analysis and quantitative assessment: Qualitative analysis: Identifying areas with obvious classification errors through visual interpretation of the classification maps; Quantitative assessment: Using the GEE platform to generate confusion matrices and calculate metrics such as User's Accuracy (UA), Producer's Accuracy (PA), Overall Accuracy (OA), and the Kappa coefficient to comprehensively measure classifier performance.

Table 4. Random Forest classification schemes based on different feature inputs (Models 1–5)

Model	Data Type	Temporal Strategy	Features Used	Phenology Division
1	Radar only	Monthly median	Radar indices	✗
2	Optical only	Monthly median	Optical indices	✗
3	Optical + Radar	Monthly median	Optical + Radar indices	✗
4	Optical only	Phenology-based	Optical indices	✓
5	Optical + Radar	Phenology-based	Optical + Radar indices	✓

4. Results

4.1. Spectral Separability

Figure 3 shows the JM distance results between garlic and wheat under different phenological stages and their combinations.

At a single phenological stage, the JM distance is lowest during the germination stage, only 0.14, indicating that the spectral difference between the two is minimal at this stage; whereas from the regreening to rapid growth stage, the JM distance is the highest, reaching 1.40, indicating the best discriminative effect. This is mainly caused by two factors: first, during this stage, both garlic and wheat enter the canopy closure period, but wheat grows faster and has stronger photosynthesis, resulting in a significant increase and right-shift in red-edge reflectance, which enlarges the red-edge difference between the two; second, in terms of visible light, garlic leaves are overall green, while wheat has higher chlorophyll content, appearing dark green. The difference in their vegetation indices (such as GCVI, S2REP) responses is further amplified, enhancing their separability.

In the combination of multiple phenological stages, when integrating year-round phenological information (PP1-6), the JM distance is the highest at 1.85, indicating that combining year-round features can maximize crop distinguishability. It is worth noting that when only using stages 1–5, the JM distance also reaches 1.83, close to the year-round combination. This suggests that as long as coverage extends to before the end of the rapid growth period (e.g., before mid-April), high classification accuracy can still be achieved even without imagery from the maturity period, which has practical reference value for situations where image acquisition is limited or for early mapping.

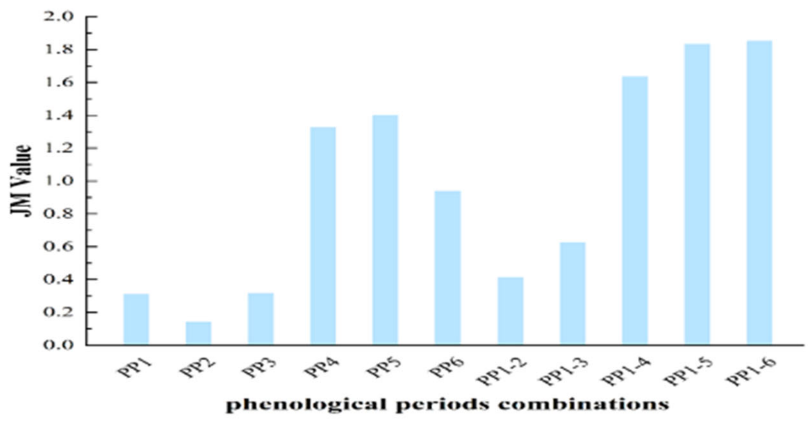

Figure 3. J-M statistics of 11 phenological period combinations between winter wheat and garlic in Kaifeng.

4.2. Classification Accuracy

To verify the accuracy of PPSF, this study conducted both quantitative and qualitative evaluations.

4.2.1. Quantitative Evaluation

Table 5. Confusion Matrix-Based Accuracy Metrics Table

Model	Sample Count	TP	FN	FP	TN	PA	UA	OA	Kappa
1	335	56	19	30	249	74.67	65.13	71.34	0.64
2	319	62	9	11	237	87.32	84.93	83.70	0.79
3	321	58	1	8	254	98.31	87.88	90.65	0.88
4	319	67	6	6	240	91.78	91.78	89.97	0.87
5	322	76	3	4	239	96.2	95	96.27	0.95

The evaluation results of confusion matrices for each model are shown in Table 5. Due to differences in cloud masks and temporal coverage across different synthesis schemes, the number of valid samples involved in classification varied slightly. The overall accuracy (OA), user accuracy (UA), and producer accuracy (PA) of PPSF in extracting garlic were 94.32%, 97.44%, and 96.20%, respectively, and the accuracies for other land cover types were also all above 85%. There was a noticeable confusion between Class 3 and Class 4, mainly because the land cover types included in these two classes were relatively complex.

4.2.2. Qualitative evaluation

Figure 4 shows the classification results of PPSF (10 m resolution). To further verify the accuracy, four randomly selected 1 km × 1 km grids within the study area were used for comparative analysis.

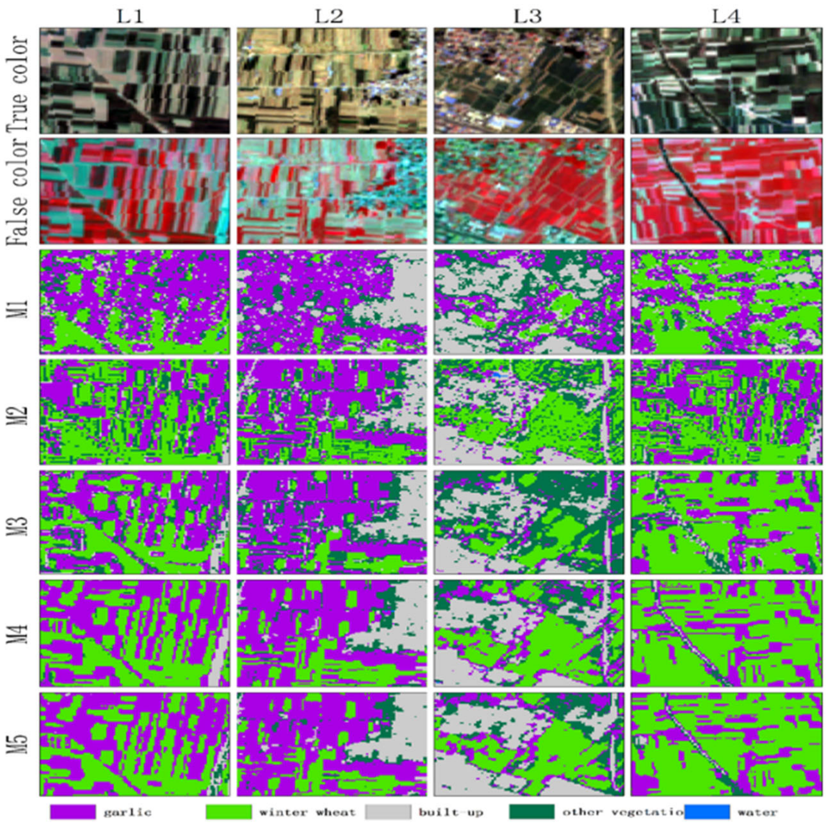

Figure 4. Classification results of different feature set

From the classification results of the four typical plots (L1–L4), different combinations of features and temporal compositing methods significantly affected garlic recognition. After introducing phenological information and integrating optical and SAR data, the classification results showed noticeable improvements in plot integrity, boundary clarity, and category confusion.

In the models using monthly composited features (M1–M3), the classification results had more noise and misclassifications. M1 (monthly compositing + SAR) showed severe confusion between garlic and winter wheat, with poor plot continuity; M2 (monthly compositing + optical) still had salt-and-pepper noise; M3 (monthly compositing + optical + SAR) improved, indicating that multi-source data fusion helps enhance separability.

After introducing phenological information, the classification results were further optimized. M4 (phenological compositing + optical) had higher spatial consistency and enhanced plot connectivity, indicating that phenological stage features can better reflect the spectral differences during key crop growth stages. M5 (phenological compositing + optical + SAR) had the best performance, with clear plot boundaries, minimal internal noise, and high consistency with the actual distribution, demonstrating that combining phenological features with SAR data better captures crop structure and water content characteristics.

In summary, phenology-based feature construction more effectively characterizes the garlic growth cycle than monthly compositing. The fusion of optical and SAR data provides complementary information, improving model stability and spatial consistency. The combination of "phenological compositing + optical + SAR" showed the best performance, confirming the advantages of multi-source phenological features in garlic remote sensing recognition.

5. Conclusion

This study proposed a method for extracting garlic planting structure by integrating optical remote sensing and SAR, combining optical and SAR imagery and using phenological features for high-precision classification of garlic in Kaifeng City. Experimental results show that the overall classification accuracy of this method exceeds 0.9, demonstrating good stability and reliability. The success of the method lies in its ability to divide phenological periods based on active and passive remote sensing time series, accurately capturing the key characteristics of the garlic growth cycle; at the same time, the integration of optical and SAR imagery compensates for the limitations of a single data source under weather or seasonal conditions, achieving complementary advantages. In addition, integrating features across the whole growth period fully utilizes the spectral and structural information of each phenological stage, enhancing overall discriminative ability. In summary, the proposed method can achieve high-precision garlic classification and has good generalizability, providing a reference for agricultural production management and crop monitoring. Future research can further explore object-oriented or deep learning techniques to improve classification accuracy and applicability.

Acknowledgements

Natural Science Foundation.

References

[1] Mo X, Liu S, Lin Z, et al. Regional crop yield, water consumption and water use efficiency and their responses to climate change in the North China Plain[J]. Agriculture, Ecosystems & Environment, 2009, 134(1-2): 67-78.

[2] Liu L, Xiao X, Qin Y, et al. Mapping cropping intensity in China using time series Landsat and Sentinel-2 images and Google Earth Engine[J]. Remote Sensing of Environment, 2020, 239: 111624.

[3] Kuang Wenhui, Zhang Shuwen, Du Guoming, et al. Remote sensing mapping and spatiotemporal feature analysis of land use change in China from 2015 to 2020[J]. Acta Geographica Sinica, 2022: 1-16.

[4] CHEN Q, CAO W, SHANG J, et al. Superpixel-Based Cropland Classification of SAR Image With Statistical Texture and Polarization Features[J/OL]. IEEE Geoscience and Remote Sensing Letters, 2022, 19: 1-5.

[5] USEYA J, SHENGBO C. Exploring the Potential of Mapping Cropping Patterns on Smallholder Scale Croplands Using Sentinel-1 SAR Data[J/OL]. Chinese Geographical Science, 2019, 20(4): 626-639.

[6] imagery for surface water mapping applications[J/OL]. Results in Physics, 2018, 9: 275-277.

[7] Shi Lei, Yang Liangyan, Wang Kun, et al. Monthly temperature vegetation drought index dataset in the Loess Plateau region from 2000 to 2024 [J/OL]. Chinese Science Data (Chinese and English Online Edition), 1-17 [2026-03-24]. https://link.cnki.net/urlid/11.6035.N.20260318.1608.011.

[8] Qiu Xinxin, Wang Chunmei, Yang Jian, et al. Evaluation study on quantitative estimation of land surface soil moisture using domestic "Gaofen-3" SAR series satellites [J]. Aerospace Return and Remote Sensing, 2026, 47(01): 83-99.

[9] Han J, Zhang Z, Cao J, et al. Mapping rapeseed planting areas using an automatic phenology- and pixel-based algorithm (APPA) in Google Earth Engine [J]. The Crop Journal, 2022, 10(05): 1483-1495.

[10] Teluguntla P, Thenkabail P S, Oliphant A, et al. A 30-m landsat-derived cropland extent product of Australia and China using random forest machine learning algorithm on Google Earth Engine cloud computing platform [J]. ISPRS Journal of Photogrammetry and Remote Sensing, 2018, 144: 325-340.

[11] Guo Zhen, Zhang Qi, Liu Dazhao. Scale effect of mangroves under multi-source remote sensing collaboration [J/OL]. Journal of Hainan Tropical Ocean University, 1-15 [2026-03-24]. https://link.cnki.net/urlid/46.1085.G4.20260311.2114.002.

[12] Ni R, Tian J, Li X, et al. An enhanced pixel-based phenological feature for accurate paddy rice mapping with Sentinel-2 imagery in Google Earth Engine [J]. ISPRS Journal of Photogrammetry and Remote Sensing, 2021, 178:282-296. DOI:10.1016/j.isprsjprs.2021.06.018.

[13] E Hailin, Zhou Decheng, Li Kun. Method for extracting the planted area of rice based on Sentinel 1/2 and GEE—A case study of Hangjiahu Plain [J]. Intelligent Agriculture (Chinese and English), 2025, 7(02):81-94.

[14] HUANG H, LEGARSKY J, OTHMAN M. Land-cover classification using Radarsat and Landsat imagery for St. Louis, Missouri [J/OL]. Photogrammetric Engineering and Remote Sensing, 2007.

[15] Li W, Pan J, Peng W, et al. Mapping Garlic Crops and Change Analysis in the Erhai Lake Basin Based on Google Earth Engine [J]. 2024. DOI:10.20944/preprints202402.1216.v1.

[16] Soudani K, Delpierre N, Berveiller D, et al. Potential of Synthetic Aperture Radar Sentinel-1 time series for the monitoring of phenological cycles in a deciduous forest [J]. International Journal of Applied Earth Observation and Geoinformation, 104 [2026-03-24]. DOI:10.1101/2021.02.04.429811.

[17] Guo Y, Xia H, Zhao X, et al. Estimate the earliest phenophase for garlic mapping using time series Landsat 8/9 images[J]. Remote Sensing, 2022, 14(18): 4476.

[18] Guo Y, Xia H, Zhao X, et al. Early-season mapping of winter wheat and garlic in the Huaihe Basin using Sentinel-1/2 and Landsat-7/8 imagery[J]. IEEE Journal of Selected Topics in Applied Earth Observations and Remote Sensing, 2022, 16: 8809-8817.

[19] Tian H, Yang M, Wu F, et al. Potential of Landsat-9 for early-season mapping of winter garlic and winter wheat[J]. Geo-spatial Information Science, 2024, 27(6): 2199-2210.